Research papers

A fast dynamic model for a large scale heat pipe embedded latent heat thermal energy storage system for optimal sizing and control

Chunjian Pan [a], Natasha Vermaak [a], Xingchao Wang [b,c,*], Carlos Romero [a], Sudhakar Neti [a], Chien-Hua Chen [d], Richard Bonner [d]

[a] Energy Research Center, Lehigh University, Bethlehem, PA 18015, United States
[b] Department of Mechanical Engineering, Colorado School of Mines, 1500 Illinois St., Golden, CO 80401, United States
[c] National Renewable Energy Laboratory (NREL), 15033 West Denver Pkwy, Golden, CO 80401, United States
[d] Advanced Cooling Technology, Inc., 1046 New Holland Ave Building 2, Lancaster, PA 17601, United States

ARTICLE INFO

ABSTRACT

One of the challenges to design and control phase change material (PCM) based latent heat thermal energy storage (LHTES) systems is to develop fast models to accurately represent their transient and nonlinear behaviors. In this paper, a fast explicit modeling approach for a multi-dimensional finned PCM system, called alternating front propagating, is proposed based on the concept of the alternating-direction implicit algorithm for multi-dimensional parabolic and elliptic differential equations. The proposed modeling method is employed to develop a fast explicit dynamic model for a large scale LHTES system, whose heat transfer is enhanced by imbedded circular finned heat pipes. The developed fast model has negligible computational cost and is of sufficient accuracy compared to high-fidelity numerical solutions. The fast explicit model of the LHTES system was employed in a model predictive control framework to determine the HTF flowrate so that its outlet temperature meets a target value. The controlled HTF flowrate can increase the usage efficiency of the stored heat in a LHTES system.

1. Introduction

LHTES systems based on phase change materials (PCM) have two obvious advantages over sensible thermal energy storage for many applications. One is higher energy density, resulting in smaller equipment size and less investment cost. The other is isothermal heat releasing/absorbing, resulting in efficient temperature management. Despite the advantages LHTES systems also have several engineering challenges. The low conductivity of PCMs is one barrier preventing wide commercial applications [1,2]. Using nanofluids is one potential technique to increase equipment heat transfer [3,4]. To offset the low conductivity of PCMs, design of fins is often being studied to enhance the heat transfer performance of a LHTES system [5]. Adding fins was reported to be less expensive than other techniques to due to their relatively simpler manufacture process [6,7]. Embedding heat pipes acting as high conductivity fins is popular strategy to increase the heat transfer performance for different applications [8–12]. A heat pipe assisted LHTES system is a convenient configuration for large scale applications, e.g., the concentrating solar power field [8,9].

Another application barrier is the difficulty of developing low cost computational models for a LHTES system for optimal sizing and operation control. The design of LHTES systems is often based on parametric studies using high computational cost models with various performance goals [13–25]. For example, Pirasaci et al. [13] employed the effectiveness of the storage as the design criterion and numerically studied the length of the tubes, the flow rate of the heat transfer fluid (HTF), diameter of a tube and distances between tubes on the effectiveness of a shell-and-tube based LHTES system. Zheng et al. [16] numerically studied the optimal eccentricity between inner and outer tubes of a shell-and-tube based LHTES system to decrease the melting/solidification time. Exergy efficiency is also employed as a design metric for geometric parameter design in [18,23,24]. Maximized exergy was used as design metric by Tang et al. [25]. In summary, there is lack of a unanimous design protocol and different design targets such as effectiveness, thermal storage efficiency, solidification time, heat transfer rate and exergy maximization are employed as performance indicators.

In the above design review, two common operational variables are: the inlet temperature and mass flow rate of the HTF going through a LHTES system for heat exchange. Qu et al. [26] experimentally studied

---

Nomenclature

c_p	heat capacity, J/kgK
h	melting front along the vertical direction, cm
h_0	PCM height on each circular plate, cm
h_g	air gap between the PCM and the circular fin, cm
h_f	convective heat transfer coefficient in the HTF channel, W/m^2K
h_{hp}	effective convective heat transfer coefficient of a heat pipe, W/m^2K
H	height of the HTF channel, m
k_f	conductivity of HTF, W/mK
k_{pcm}	conductivity of PCM, W/mK
L	latent energy, kJ/kg
N_x	number of heat pipes in a row perpendicular to the flow direction
N_y	number of circular plate fins along the height of a heat pipe
N_z	number of heat pipe rows along the flow direction
q_f	mass flow rate of the HTF, *kg/s*
Q	accumulated energy in the HTF, MJ
r	melting front along radial direction, cm
r_1	radius of heat pipe, cm
r_2	outer radius of the annular plate fin, cm
R_1	thermal resistance of the PCM along the radial direction, K/W
R_2	thermal resistance of the PCM along the vertical direction, K/W
R_t	total thermal resistance
T_m	phase change material (PCM) melting temperature, °C
T_{hp}	heat pipe inner temperature, °C

T_w	heat pipe wall temperature, °C
T_{int}	interface temperature between HTF and the heat pipe, °C
V	PCM volume, m^3
w_{fin}	thickness of bottom circular fin, mm
w_t	thickness of a heat pipe wall, mm
W	width of the tank LTES system, m
Y	height of the HTF channel, m
Z	length of the HTF channel or the tank LTES system, m

Greek letters

ρ	density, kg/m³
μ	viscosity, μPa · s
Δ	incremental step change

Superscripts

i	discrete location
k	discrete time step

Subscripts

pcm	phase change material
f	heat transfer fluid (HTF)
hp	heat pipe
fin	bottom circular fin
in	inlet conditions of HTF
out	outlet conditions of HTF

Acronym

HTF	heat transfer fluid
LHTES	latent heat thermal energy storage
PCM	phase change material

the employment of a LHTES based reverse cycle for air source heat pump defrosting. It was found that the heat distribution pattern was mainly influenced by the refrigerant flow rate and therefore the flow rate control is an effective way to regulate the heat distribution within the system. There is limited number of studies on operational research of a large scale LHTES system in the literature. However, as application processes with energy storage are inherently transient [27,28], e.g., solar thermal systems, heating, ventilation and air condition (HVAC) systems in buildings, operational strategies for effective dynamic heat management are needed [29].

The inherent nonlinearity and transient charging/discharging of a LHTES system are the key characteristics that complicate the formulation of a fast dynamic model for control applications. The melting/solidification process coupling with the HTF flow channels is described by a set of nonlinear partial differential equations (PDEs). This means after discretization of the geometry, at each time step, a large scale nonlinear system of equation to be solved. When natural convection is to be taken into consideration during the melting process, which requires fine mesh to ensure the convergence of the momentum equation, the numerical process for optimization purpose would become intractable. A thermal network model was developed by Shabgard et al. [8] to predict the performance of a LHTES system with cascaded PCMs based on exergy analysis. A dynamic numerical model based on a thermal resistance network was developed by Nithyanandam & Pitchumani [9] to study the influence of design and operating parameters on the charge and discharge performance of a large scale LHTES system. However, the thermal network models developed in [8,9] still require solving large coupled system of governing equations. As a result, the computational efficiency of these models is not sufficient for operational research purposes.

The optimal operational strategies could result in substantial investment savings for a large scale system. A fast and accurate dynamic model for control applications is critical [30–39]. A control oriented dynamic model for a LHTES unit coupled with a solar thermal collector and a backup electric heater was developed by Serale et al. [30] for space heating. A mixed logic-dynamical approach was introduced to regulate the system with intrinsic nonlinearities. With the aim to efficiently model the non-linear operational characteristics of a LHTES system, Ghani et al. [31] built a dynamic model by using a Layered Digital Dynamical Neural network which was trained with experimental data obtained from a LHTES system. Luu et al. [32] proposed integrating a LHTES system into a domestic solar water heater to eliminate the traditional water tank. A dynamical model for process operation analysis was developed and validated against experimental data. To monitor safe operation of lithium-ion battery packs coupled with phase change composites for passive cooling, Salameh et al. [33] developed a state-space dynamical model to estimate the melt fraction of the stored latent cooling energy in the system. Barz et al. [34] developed a nonlinear state observer based on a physical 2-D dynamic model to reconstruct transient spatial temperature fields inside the storage and estimate the stored energy and the state of charge.

A fast dynamic model is the most challenge and essential to facilitate operational study of a LHTES system [30–34]. In this paper, a fast discrete-time dynamic model was proposed for a large scale LHTES system. First a fast PCM solidification model is developed based on the concept of alternating-direction implicit method [35] for a 2-D cylindrical PCM unit as a module, which is extension of the work [36] for PCM solidification/melting front propagates from 1-D to 2-D. The whole LHTES system is composed of these modules and the overall system behavior are updated interactively between the HTF channel and the PCM domain through boundary conditions and energy balance without solving a system of equations. With such proposed techniques, the nonlinear dynamical behavior is able to be described by a series of explicit algebraic equations, which greatly reduces the computational

burden when employed as a dynamical system model for operational design studies and model predictive control.

The content of this paper is organized as follows. In Section 2, a fast explicit dynamic model for a circular finned heat-pipe embedded PCM module is constructed based on alternating solidification front propagating. In Section 3, the module model developed in Section 2 is employed to construct a fast dynamic for a large-scale LHTES system. In Section 4 the fast dynamic model of a large-scale LHTES system is used for design analysis and for a HTF flow rate regulation problem. Section 5 summarizes the conclusions.

2. A fast explicit dynamic model for a finned heat pipe embedded PCM module

The fundamental basis of developing a fast dynamic model is based on thermal resistance analysis. In general, thermal resistance is defined under steady-state heat transfer conditions. With the following two assumptions, thermal resistance network based modeling approach is applicable to PCM systems. One critical assumption is that the PCM solidifies at a constant temperature. Another one is that the temperature gradient is linear within the solidified PCM domain from the boundary to the solidification front. The second assumption sacrifices the accurate account of the sensible energy, but the latent energy dominates the total energy of the system, so it is reasonable. One more key assumption being used to derive a fast model is that the heat transfer within PCM is conduction based. If natural convection was to be considered in the melt PCM, fine mesh would be required to ensure convergence of the momentum equation and hence resulting in a high computational model. For the solidification process, conduction based models were reported to have good agreement between experiments and simulations such as by Ammar [41]. Studies [42–44] showed that the employment of an effective thermal conductivity can successfully account for convection in the melt PCM during melting.

2.1. Alternating front propagating for PCM solidification

A fast explicit modeling approach, called alternative front propagating, is introduced in this section. The basic idea is that the solidification front is updated layer by layer in each main geometrical direction alternatively based on thermal resistance network. This approach borrows the concept from the alternating direction implicit method that was proposed by Peaceman et al. [35] to solve parabolic and elliptic differential equations. The method solves a multidimensional differential equation along each perpendicular space direction alternatively so that the original large-scale system of equations can be split into several smaller set of system equations that can be more efficiently solved by a direct, non-iterative method such as direction a tri-diagonal algorithm [40].
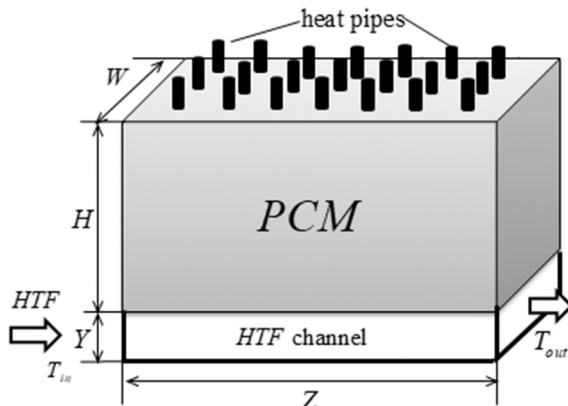
A heat pipe assisted large scale LHTES system is shown in Fig. 1. Heat pipes are embedded in the PCM tank and connected to a heat transfer fluid (HTF) channel. The application of such a LHTES is reported in [48]. Annular fins are attached to a single heat pipe as shown in Fig. 2. Solid PCM sinks down to the bottom of a heated plate during melting, so a circular plat fin effectively promotes heat transfer utilizing contact melting behavior [47]. For a heat pipe, it is reasonable to assume that there is no temperature drop along its length [49], so the transient PCM behavior on a single annular extended fin (see Fig. 3) can be used to represent a whole tube.

It should be noted that a simplified model was developed for this same geometry in [48], where a data-driven correction factor was introduced to adjust the total solidification time of a 2-D cylindrical PCM-container module. The simplified model in [48] uses a data-driven tuning factor to correct a simplified transient thermal resistance model. In this paper, by updating the melting/solidification front alternatively in each direction, reasonably accurate results compared to detailed numerical solutions can be obtained without using a tuning factor. Hence the novel modeling method introduced in this paper is an upgrade of the method in [48].

Although temperature drop in a heat pipe can be neglected, in the following description, a thermal resistance of a heat pipe (R_{hp}) is nevertheless introduced to generalize the mathematical model. Thus an inner heat pipe temperature T_{hp} and heat pipe wall temperature T_w are also introduced. Based on the concept of thermal resistance networks for heat flow, the heat coming from the heat pipe into the PCM can be written as:

$$\frac{T_{hp} - T_w}{R_{hp}} = \frac{T_w - T_m}{R_1} + \frac{T_w - T_m}{R_{fin} + R_2} \tag{1}$$

where R_1 and R_2 are the thermal resistances within the bulk PCM along the radial and vertical directions respectively; R_{fin} is the thermal resistance in the bottom circular fin. The two terms at the right side of the equation represents two paths for heat coming from the pipe and going into the PCM. This is a key approximation being used to derive a fast model to capture the essential dynamics of the heat transfer process. Based on Eq. (1), the wall temperature of the heat pipe is:

$$T_w = \frac{R_1\left(R_{fin} + R_2\right)T_{hp} + R_{hp}\left(R_{fin} + R_2\right)T_m + R_1 R_{hp} T_m}{R_1\left(R_{fin} + R_2\right) + R_{hp}\left(R_{fin} + R_2\right) + R_1 R_{hp}} \tag{2}$$

The total thermal resistance from the heat pipe to the moving fronts of

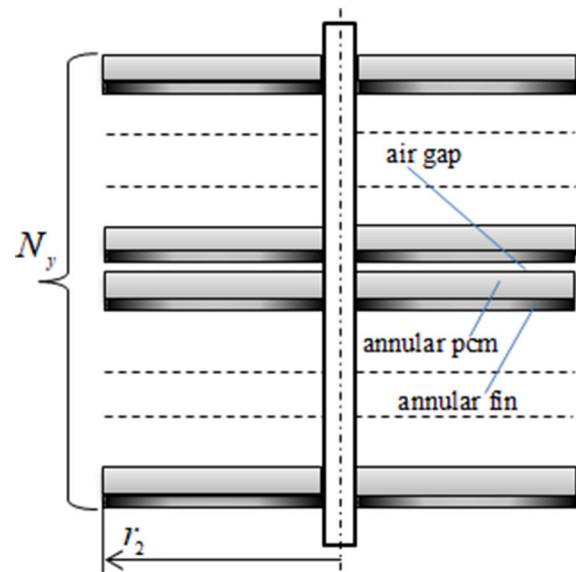**Fig. 1.** Schematic of a large scale LHTES system with embedded heat pipes.

Fig. 2. Cross-sectional schematic of a single heat pipe unit with annular fins.
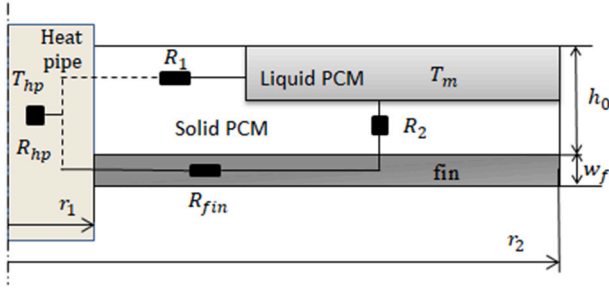
Fig. 3. Schematic of annular finned PCM unit of a heat pipe.

the PCM can be written as:

$$R_t = R_{hp} + \frac{R_1 + R_2 + R_{fin}}{R_1 (R_{fin} + R_2)},\qquad(3)$$

which is a transient variable, as R_1 and R_2 depends on the moving fronts of the PCM.

The idea of alternating front propagating is to update the solidification front alternatively between the radial and the vertical directions. The two directions are perpendicular to each other, which is a basic requirement for the alternating updating strategy and is introduced as follows.

Beginning from the radial direction, it is assumed that the heat flow into the PCM within a small time window Δt is equal to the latent energy change happening in a small radial distance Δr, thus an energy balance equation using the thermal resistance network can be written as:

$$\frac{T_w - T_m}{R_1} = \frac{\rho_{pcm} 2\pi r^{k-1} \Delta r^k h^{k-1} L_{pcm}}{\Delta t}.\qquad(4)$$

where h^{k-1} and r^{k-1} represent the solidification front at the previous time step along the vertical and radial directions, respectively. L_{pcm} is the latent heat of the PCM and ρ_{pcm} denotes the PCM density. Consequently, the incremental marching melt front at the time k is:

$$\Delta r^k = \frac{(T_w - T_m)\Delta t}{R_1 \rho_{pcm} 2\pi r^{k-1} h^{k-1} L_{pcm}}\qquad(5)$$

Hence the moving melt front in the radial direction is updated as:

$$r^k = r^{k-1} + \Delta r^k\qquad(6)$$

Similarly, along the vertical direction, the energy balance equation is:

$$\frac{T_w - T_m}{R_{fin} + R_2} = \frac{\rho_{pcm} \pi \left(r_2^2 - (r^k)^2\right) \Delta h^k L_{pcm}}{\Delta t}\qquad(7)$$

Thus, the incremental melt front along the vertical direction at the time k with the updated melt front r^k can be obtained as:

$$\Delta h^k = \frac{(T_w - T_m)\Delta t}{(R_{fin} + R_2)\rho_{pcm} \pi (r_2^2 - (r^k)^2) L_{pcm}}\qquad(8)$$

The distance of the solidification front away from the annular fin along the vertical direction is updated as:

$$h^k = h^{k-1} + \Delta h^k\qquad(9)$$

Generally, this discrete-time dynamic model can be written as:

$$[h^k, r^k, R_t^k] = F\left(T_f^k, \Delta t^k\right)\qquad(10)$$

where R_t^k (Eq. (3)) is the total thermal resistance, which is transient and depends on the propagation of h^k and r^k. The following lists the calculations of the thermal resistances. The thermal resistances within the PCM are updated according to the moving fronts h^k, r^k, and they can be expressed as:

$$R_1^k = \frac{log(r^k/r_1)}{2\pi(h_0 - h^k)k_{pcm}}\qquad(11)$$

$$R_2^k = \frac{h^k}{\pi\left[(r_2)^2 - (r^k)^2\right]k_{pcm}}.\qquad(12)$$

The thermal resistance of the fin is:

$$R_{fin} = \frac{log(r_2/r_1)}{2\pi w_{fin} k_f}.\qquad(13)$$

The thermal resistance in the heat pipe includes the wall conduction resistance and effective convection heat transfer resistance:

$$R_{hp} = \frac{1}{2\pi r_1(w_f + h_0)h_{hp}} + \frac{log(r_1/(r_1 - w_t))}{2\pi(w_f + h_0)k_f},\qquad(14)$$

where h_{hp} is the effective heat transfer coefficient of the heat pipe and w_t is the tube wall thickness. The thermal resistance of a heat pipe is negligible [49] (h_{hp} has a large value), so its dynamics is very fast compared to transient thermal behavior of PCM. Therefore, a steady-state resistance model is a reasonable approximation for a heat pipe.

2.2. Model verification

For a set of 8 testing cases (Table 1), computational fluid dynamics solutions were found using the Solidification & Melting Model in FLUENT. The validation of the modeling package for a solidification process is reported in the literature [45,46]. A detailed Fluent model description, as well as mesh and time-step independence studies that are close to the current numerical cases can be found in [48]. The numerical results of the testing cases (Table 1) are used to verify the applicability of the fast explicit model outlined in Section 2, which was coded in MATLAB.

Note that the first 4 test cases have different geometries (i.e., ratios $\frac{r_2}{r_1}$, $\frac{h_0}{r_1}$) but the same boundary conditions, while the last 4 cases have different boundary conditions, fin thicknesses and properties. Fig. 4 shows the comparison between the fast explicit model ('FEM') and the numerical results by Fluent ('num.') for the 8 testing cases. Overall, the fast model agrees very well with the transient freezing curve determined by the Fluent simulations (within 15% for the worst case in terms of final freezing time).

Based on the testing cases (Fig. 4a), a confident working range for the ratio $\frac{r_2}{r_1}$ is $4 \leq \frac{r_2}{r_1} \leq 12$. The lower bound may not have to be specified, because when $\frac{r_2}{r_1}$ is small, heat transfer from the tube wall dominates. Cases # 5–8 have the same dimensions, but different boundary conditions, fin thicknesses and properties. It can be seen that the fast models perform quite well under variations of those parameters (with only a maximum of 6% difference exhibited in terms of final freezing time). Thus besides its dynamical performance tracking, the RDM can also be used for optimal dimensional design of LHTES systems (Fig. 1) with embedded annular finned heat pipes.

Table 1
Test cases.

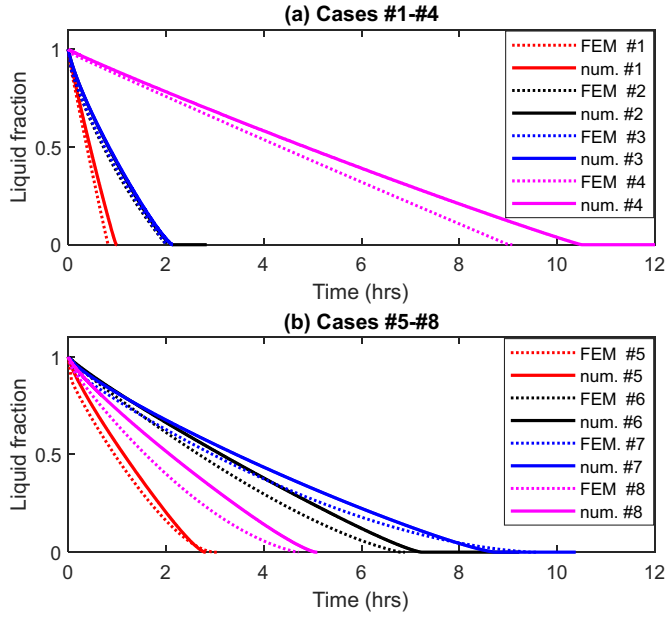| Cases	r_1 (cm)	r_2 (cm)	h_0 (cm)	w_{fin} (mm)	h_{hp}	dT (°C)	Fin
#1	0.5	2.0	0.25	0.5	350	10	Steel
#2	0.5	2.0	6.0	0.5	350	10	Steel
#3	0.5	2.0	10.0	0.5	350	10	Steel
#4	0.5	6.0	0.25	0.5	350	10	Steel
#5	0.5	3.0	2.0	0.25	350	20	Steel
#6	0.5	3.0	2.0	1.0	150	10	Steel
#7	0.5	3.0	2.0	0.5	500	5	Steel
#8	0.5	3.0	2.0	0.25	350	10	Al

Fig. 4. Testing cases used in verifying the fast model against Fluent simulations.
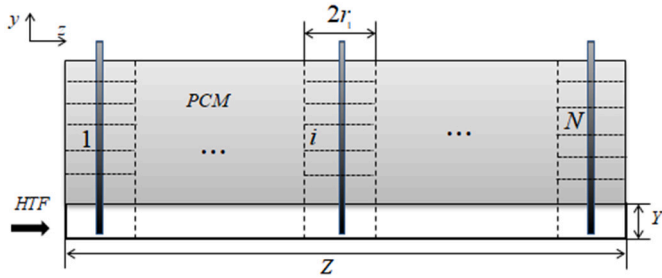

Fig. 5. A shell and tube latent energy storage unit.

3. A fast explicit dynamic model for a large scale LHTES system

A typical numerical approach of the LHTES system is simulated the HTF domain and the PCM domain in a coupled manner [17]. Due to the nonlinearity and transient behaviors of PCM solidification/melting, the system is described by a set of nonlinear partial differential equations. This means after moderate discretization of the geometry, at each time step, a large scale nonlinear system of equations is to be solved. Such a numerical approach would exert a huge computational burden to carry out thorough operational studies of a LHTES system. In Section 2, an explicit fast dynamical model for a heat pipe unit was developed. In this section, a modeling approach to develop a dynamic model for a whole LHTES system using the fast model as a module is presented.

Given an inlet temperature of the HTF, time-implicit discretization (backward Euler method) of the transient energy balance equation of the HTF ensures stability of the numerical solution, while the up-wind finite difference scheme shows that the down-stream grid point can be updated from the up-stream grid information explicitly. The two features result in a series of explicit equations with no need of solving a system of equations to stably update the temperature profiles of the HTF along the channel. Then by employing the explicit fast model of a finned heat pipe embedded PCM module and updating the overall system behavior interactively between the HTF channel and PCM domain through energy balance boundary conditions, no solving a system of equations is required. With such proposed techniques, the nonlinear dynamical behavior is able to be described by a series of explicit

algebraic equations, resulting in a fast dynamic model for the large-scale storage system.

For a mathematical description of the fast modeling approach, the following assumptions are made: (1) the HTF is incompressible and viscous dissipation is negligible; (2) the HTF is uniform over the cross sectional area; (3) heat transfer along the HTF flow direction is negligible; (4) heat transfer in the PCM is conduction controlled; (5) the outer wall of the PCM is adiabatic; (6) PCM properties are constant; (7) the channel wall thickness is neglected, thus no thermal resistance of the wall is considered; (8) the heat pipes pass through the PCM tank and almost reach the bottom of the HTF channel.

Within the channel, it is assumed the HTF only transfers heat with the immersed section of the heat pipes. In each annular finned module, there is an air gap between two neighboring modules; this gap is reserved for PCM expansion (see Fig. 2). This air gap prevents heat transfer from a lower annular finned PCM unit to an upper one. Therefore, only the very bottom annular finned PCM unit can be heated by the upper HTF channel surface. Thus it is justified to assume that the HTF only transfers heat to the PCM through the immersed section of the heat pipes within the channel. Based on the above assumptions, the governing equation for energy transfer of the HTF in the tube is:

$$\rho_f c_{pf} YW\Delta Z\left(\frac{\partial T_f}{\partial t} + u\frac{\partial T_f}{\partial z}\right) = 2\pi r_1 YN_x h_f\left(T_{int} - T_f\right),\tag{15}$$

where h_f is the heat transfer coefficient based on correlation equations for cross flow [32]; r_1 is the radius of the heat pipe; Y is the height of the HTF channel; N_x is the number of heat pipes in a row perpendicular to the flow direction; ΔZ is the discrete distance accounting for the number of rows of heat pipes. T_{int} acts as the interface temperature between the HTF in the channel and the heat pipe.

In the following, by employing the explicit fast dynamic model for a heat pipe module developed in Section 2, an explicit fast numerical approach that does not require the solution of any systems of equations for the modeling of the large scale LHTES system (Fig. 1), is proposed.

Fig. 6 shows a discrete unit composed of a single heat pipe. Multiple heat pipes along the flow direction can also be grouped as one discrete unit for the large scale LHTES system shown in Fig. 1. The following analysis is based on one row of heat pipes as a discrete unit. The thermal resistance of the ith discrete unit depends on the moving freezing fronts of $r^{i,k}$, $h^{i,k}$ at time k and is written as:

$$\left[h^{i,k}, r^{i,k}, R_t^{i,k}\right] = F\left(T_{int}^{i,k}, \Delta t^k\right)\tag{16}$$

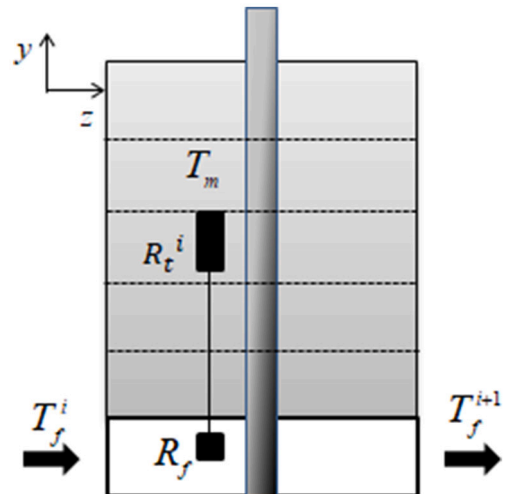Between each time interval, the volume of PCM turning from liquid to solid can be calculated as:

Fig. 6. Thermal resistance scheme of element i based on Fig. 5.

$$V^{i,k} = \pi\left(r_2^2 - r_1^2\right)h^k + \pi\left(\left(r^{i,k}\right)^2 - r_1^2\right)\left(h_0 - h^k\right) \tag{17}$$

$$V^{i,k-1} = \pi\left(r_2^2 - r_1^2\right)h^{k-1} + \pi\left(\left(r^{i,k-1}\right)^2 - r_1^2\right)\left(h_0 - h^{k-1}\right) \tag{18}$$

$$\Delta V^{i,k} = V^{i,k} - V^{i,k-1}. \tag{19}$$

The latent energy transfer associated with this volume change transfers to the HTF channel; an energy balance equation for a discrete unit with one row of heat pipes perpendicular to the flow direction can be written as:

$$2\pi r_1 Y N_x h_f \left(T_{int}^{i,k+1} - T_f^{i,k+1}\right) = \frac{\rho_{pcm} L_{pcm} \Delta V^{i,k}}{\Delta t} \tag{20}$$

Then the energy balance equation in the HTF channel can also be written as:

$$\rho_f c_{pf} Y W \Delta Z \left(\frac{\partial T_f}{\partial t} + u\frac{\partial T_f}{\partial z}\right) = \frac{\rho_{pcm} L_{pcm} \Delta V^{i,k}}{\Delta t}. \tag{21}$$

Assume N_y is the total number of annular plate fins along the height of a heat pipe. Implementing an implicit scheme and using a finite difference approach for the partial differential terms, Eq. (21) becomes:

$$\rho_f c_{pf} Y W \Delta Z \left(\frac{T_f^{i,k+1} - T_f^{i,k}}{\Delta t} + u\frac{T_f^{i,k+1} - T_f^{i-1,k+1}}{\Delta Z}\right) = N_x N_y \frac{\rho_{pcm} L_{pcm} \Delta V^{i,k}}{\Delta t} \tag{22}$$

Setting $\Psi(t^k, i) = \frac{N_x N_y}{\rho_f c_{pf} Y W} \frac{\rho_{pcm} L_{pcm} \Delta V^{i,k}}{\Delta t}$, the temperature in the HTF can be updated as:

$$T_f^{i,k+1} = \frac{1}{\Delta z/\Delta t + u}\left(\Psi(t^k, i) + \frac{\Delta z}{\Delta t} T_f^{i,k} + u T_f^{i-1,k+1}\right) \tag{23}$$

The interface temperature can be obtained from Eq. (20), and it can be written as:

$$T_{int}^{i,k+1} = \frac{T_m + 2\pi r_1 Y h_f R_t^{i,k} T_f^{i,k+1}}{1 + 2\pi r_1 Y h_f R_t^{i,k}} \tag{24}$$

Due to the size limitations of an annular finned unit, in the simulation when either $h^{i,k}$ or $r^{i,k}$ reaches the boundary first, a constraint is set as:

$$\text{when } h^{i,k} \geq h_0, \text{ or } r^{i,k} \geq r_2 \ R_t^{i,k} = \infty. \tag{25}$$

The overall calculation procedure for the proposed fast explicit modeling framework is available in Appendix.

The accuracy of a single finned heat pipe embedded PCM module has been verified by high fidelity numerical simulations in Section 2.2. The same system-level modeling framework for a whole LHTES system by assembling modules was applied to a shell-and-tube based LHTES, where it was verified by a finite-volume approach [36]. Therefore, direct verification with respect to a finite-volume model for the current whole LHTES system is not conducted. Instead, energy balance check between the HTF and the PCM in the tank is performed for the system to verify the accuracy of the code. Testing cases with three different HTF channel length (Z) (Fig. 1) were considered. The detailed dimensions of the cases are listed in Table 2 and it is assumed that (i) the HTF is water (properties shown in Table 3) (ii) the HTF mass flowrate is 10 (kg/s) and (iii) the inlet temperature is 0 °C. The PCM properties used are shown in Table 4. Fig. 7 shows the output temperature profiles of the HTF going through three different channel lengths. Longer channels result in longer dwell time for the HTF, leading to higher output temperatures. The

Table 3
Properties of water.

ρ_f	k_f	c_{pf}	μ_f
988.2 (kg/m^3)	0.59846 (W/mK)	4184.1 (J/kgK)	1.0016e^{-3} (Pa · s)

Table 4
Representative thermal properties of PCM.

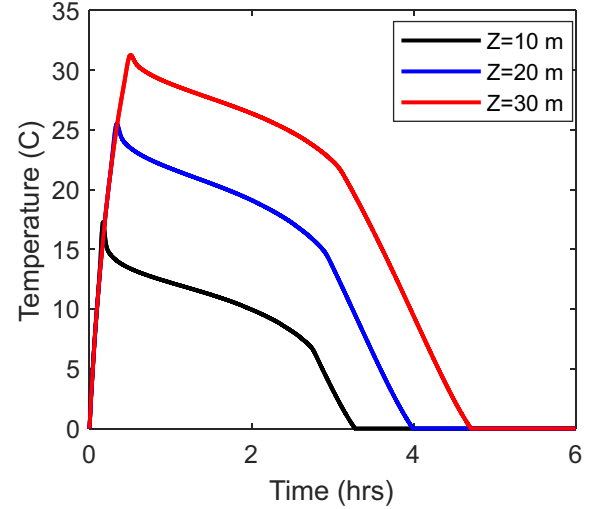| ρ_{pcm}	k_{pcm}	T_m	L_{pcm}
1538 (kg/m^3)	1.0 (W/mK)	45 (°C)	170 kJ/kg

Fig. 7. Outlet temperature of the HTF.

accumulated energy of the HTF is calculated as:

$$Q = \sum_{k=1}^{K} q_f c p_f \left(T_f^{N,k} - T_{f,in}\right)\Delta t, \tag{26}$$

where q_f is HTF inlet mass flowrate and $T_{f,in}$ is its inlet temperature. It can be seen from Fig. 8 that for the three cases, the total amount of latent energy within the PCM is balanced with the total amount of energy carried away by the HTF. Thus the modeling procedure for such a large-scale LHTES system is a reliable approximation for preliminary operational design purposes.

4. Operation of a large scale LHTES system

As it can be seen from the literature review in the Introduction that operation of a HTES system is of great importance. For a large scale LHTES system, operational strategies could be vital to improve the efficiency usage of the stored latent energy, thus reducing investment cost. With the fast explicit model developed in Section 3 for the LHTES system (Fig. 1), explore into the regulation of the mass flow rate of the HTF to increase the efficiency usage of stored heat becomes convenient.

According to Section 3, the fast explicit model for the large scale LHTES system (see Fig. 1) can be represented as:

$$T_{f,out}\left(t^k\right) = G\left(q_f\left(t^k\right), T_{f,in}\right), \tag{27}$$

Table 2
Geometries for energy balance testing.

r_1(cm)	r_2(cm)	h_0(cm)	h_g(cm)	w_{fin}(mm)	W(m)	H(m)	Y(m)	Z (m)
0.4	4	2	0.15	0.5	2	1.26	0.3	10,20,30
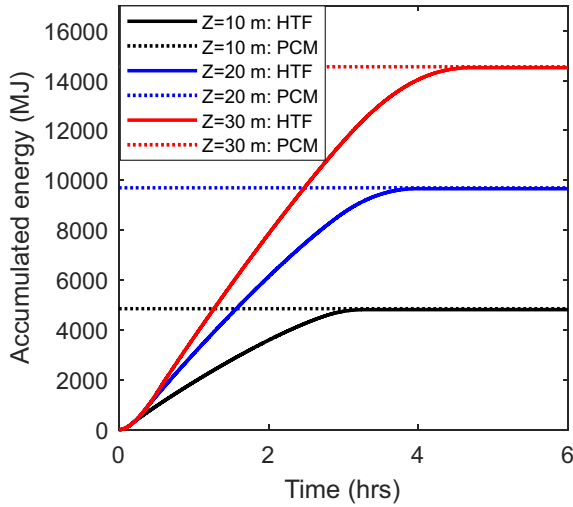
Fig. 8. Accumulated energy within the HTF.

Fig. 9. Usage efficiency versus effectiveness under HTF mass flow rates.

where $T_{f,\,out}$ is the output temperature of the HTF, q_f is the inlet HTF mass flowrate with a constant inlet temperature $T_{f,\,in}$. For the system model (Eq. (27)) to be used in the following analysis, the specific geometries of a single circular finned heat pipe are listed in Table 2 and the material properties of the HTF and the PCM are shown in Tables 3 and 4, respectively.

4.1. Effectiveness versus usage efficiency

A number of researchers have identified that the effectiveness is a useful design characteristics of a LHTES unit [33,34]. The effectiveness is defined as the ratio of the actual heat discharged over the theoretical maximum heat that can be discharged [51]:

$$\varepsilon = \frac{T_{f,out} - T_{f,in}}{T_m - T_{f,in}}. \tag{28}$$

As the effectiveness is influenced by the mass flowrate and inlet and outlet temperatures of the HTF and also directly related to the thermal resistance as explained by Tay et al. [52], there is no denial it is a useful performance indictor for system-level design.

However, one concern is that as the outlet temperature of the HTF could be dictated by the application as well as the available choice of the inlet temperature and the suitable PCMs to be used, thus the effectiveness could be result in an operational constraint that is specified by operational requirements and hence is not a good candidate as a design index. Another issue is that the effectiveness cannot reflect the usage efficiency of the stored heat when the outlet temperature of the HTF is specified as a constraint to be met. To confirm this statement, we define the usage efficiency of stored latent heat as the ratio of the used stored latent heat energy that meets the outlet temperature threshold of the HTF to the total latent heat storage capacity of the LHTES system. When the target temperature of the HTF cannot be reached, it is assumed that the remaining stored latent heat is unused.

The usage efficiency is analyzed using the numerical model (Eq. (27)). The usage efficiency as a function of effectiveness under various combinations of HTF flowrate and HTF channel length of a LHTES is shown in Fig. 9. It can be observed that when the mass flow rate of the HTF is small, the usage efficiency is high for a wide range of effectiveness. The usage efficiency is highly sensitive to the mass flow rate and decreases quickly with an increasing HTF flowrate. Even under a high effectiveness, the usage efficiency can be low due to a large HTF flowrate. Thus it suggests effectiveness is not a suitable parameter to be set as a performance indicator for design consideration. This analysis confirms that the regulation of the mass flow rate of the HTF is important to
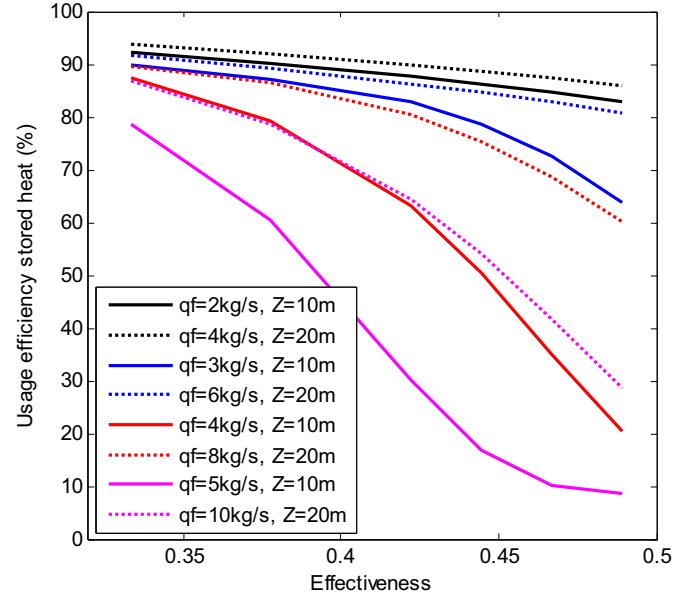
achieve high usage efficiency.

4.2. HTF flowrate control

From above analyses, it can be seen that the length of the channel and the mass flow rate of the HTF should be optimally determined in order to achieve high usage efficiency of the stored heat while meeting the required outlet temperature. Fig. 7 indicates that the output HTF temperature could decrease quickly and fail to meet the target temperature when there is not sufficient stored heat in the LHTES system. Nevertheless, there still could be a substantial amount of unused stored heat in a large-scale system (Fig. 9).

To make more efficient use of this stored heat, one solution is to reduce the flowrate of the HTF when the outlet temperature fails to meet the designed value, thus its dwell time in the LHTES system can be prolonged and its output temperature can still reach the target temperature. Under such conditions, the fast explicit model (Eq. (27)) is employed to find such a desired flowrate profile. It is assumed that the designed outlet temperature to be reached is T_d. To reach this goal, it is expressed as the cost function to minimize the deviation of the output temperature of the HTF from the design point T_d. A corresponding optimization problem can be formulated as (Eq. (28)):

$$\begin{aligned} &\underset{q_f(t^k)}{min} \quad \left(T_{f,out}(t^k) - T_d\right)^2 \\ &\text{s.t.} T_{f,out}(t^k) = G\left[q_f^{in}, T_{f,in}\right] \\ &\qquad 0 \le q_f(t^k) \le 4 \end{aligned} \tag{29}$$

When the design temperature is set at 20 °C, Fig. 10 shows the controlled inlet HTF mass flowrate profile with its output temperature profile determined by the optimal control problem. Initially the inlet HTF mass flowrate is set at $3 kg/s$. After the output temperature increases to the maximum allowable temperature, a control strategy is implemented (red section of the curves in Fig. 10) by solving Eq. (10). At the beginning there is sufficient latent energy in the LHTES system, so the inlet mass flowrate reaches its upper bound. When the remaining stored energy in the system cannot maintain the HTF output temperature at the design point, a decreasing mass flowrate is found at each discrete time window to satisfy the temperature constraint.

If no such a control strategy is implemented, the HTF outlet temperature will fail to meet a target value after 2 h (see Fig. 10a). By
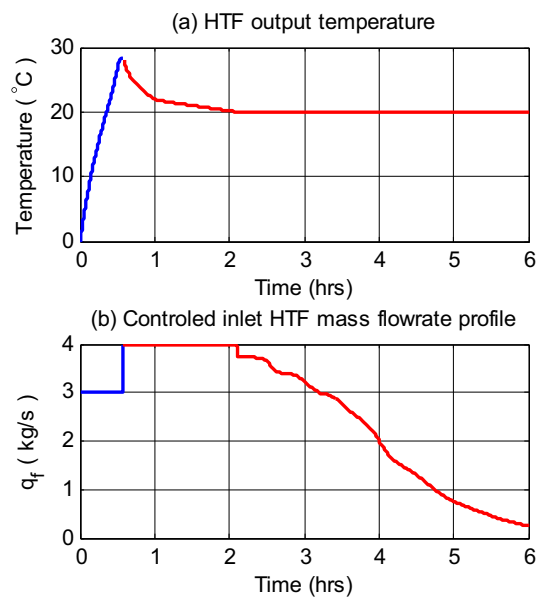
Fig. 10. Profiles of the HTF output temperature and inlet mass flow rate. (For interpretation of the references to colour in this figure, the reader is referred to the web version of this article.)

determining an optimal HTF flowrate, its outlet temperature can still be satisfied for a prolonged operation time window. As a result, more stored heat is utilized in the LHTES system, but the total heat capacity is reduced with a decreasing HTF flowrate.

5. Conclusions

In this paper, an explicit fast dynamic model for a large-scale LHTES

system is developed, whose heat transfer is enhanced by embedded circular finned heat pipes. In the proposed fast modeling approach, solidification front is updated layer by layer in each main geometrical direction alternatively based on a thermal resistance network. The proposed fast alternating PCM melting/solidification front propagating approach is generally applicable to other geometries. The model is used to control the HTF flowrate to achieve high stored heat usage efficiency under a constrained HTF outlet temperature.

CRediT authorship contribution statement

Chunjian Pan: Conceptualization, Investigation, Methodology, Formal analysis, Software, Writing – original draft. **Natasha Vermaak:** Methodology, Writing – review & editing. **Xingchao Wang:** Conceptualization, Methodology, Writing – review & editing, Validation. **Carlos Romero:** Conceptualization. **Sudhakar Neti:** Conceptualization. **Chien-Hua Chen:** Conceptualization. **Richard Bonner:** Conceptualization.

Declaration of competing interest

The authors wish to confirm that there are no known conflicts of interest associated with this publication and there has been no significant financial support for this work that could have influenced its outcome.

Appendix A

The overall calculation procedure is for the proposed fast explicit modeling framework is shown as follows, which does not involve solving any systems of equations:

First, initialize the temperature profile in the tube

$$T_f^{i,1} = T_{in}, \ T_{int}^{i,1} = T_m, \ 1 \le i \le N_z;$$

for $k = 1:K$

$$[h^{i,k}, r^{i,k}, R_t^{i,k}] = F(T_{int}^{i,k}, \Delta t^k)$$

$$if \quad h^{i,k} \ge h_0 \quad or \quad r^{i,k} \ge r_2$$

$$R_t^{i,k} = e^{15};$$

$$end$$

$$T_f^{1,k} = T_{f,in};$$

$$\Psi(t^k, i) = \frac{N_x N_y}{\rho_f c_{pf} Y W} \cdot \frac{\rho_{pcm} L_{pcm} \Delta V^{i,k}}{\Delta t};$$

$$T_f^{i,k+1} = \frac{1}{\Delta z/\Delta t + u}\left(\Psi(t^k, i) + \frac{\Delta z}{\Delta t} T_f^{i,k} + u T_f^{i-1,k+1}\right);$$

$$T_{int}^{i,k+1} = \frac{T_m + 2\pi r_1 Y h_f R_t^{i,k} T_f^{i,k+1}}{1 + 2\pi r_1 Y h_f R_t^{i,k}}$$

$$end$$

References

[1] Z.A. Qureshi, H.M. Ali, S. Khushnood, Recent advances on thermal conductivity enhancement of phase change materials for energy storage system: a review, Int. J. Heat Mass Transf. 127 (2018) 838–856.

[2] M.E. Zayed, J. Zhao, W. Li, A.H. Elsheikh, A.M. Elbanna, L. Jing, A.E. Geweda, Recent progress in phase change materials storage containers: geometries, design considerations and heat transfer improvement methods, J. Energy Storage 30 (2020), 101341.

[3] H.J. Xu, Z.B. Xing, F.Q. Wang, Z.M. Cheng, Review on heat conduction, heat convection, thermal radiation and phase change heat transfer of nanofluids in porous media: fundamentals and applications, Chem. Eng. Sci. 195 (2019) 462–483.

[4] F. Fan, C. Qi, J. Tang, Q. Liu, X. Wang, Y. Yan, A novel thermal efficiency analysis on the thermo-hydraulic performance of nanofluids in an improved heat exchange system under adjustable magnetic field, Appl. Therm. Eng. 179 (2020), 115688.

[5] A.M. Abdulateef, S. Mat, J. Abdulateef, K. Sopian, A.A. Al-Abidi, Geometric and design parameters of fins employed for enhancing thermal energy storage systems: a review, Renew. Sust. Energ. Rev. 82 (2018) 1620–1635.

[6] C. Zhao, M. Opolot, M. Liu, F. Bruno, S. Mancin, K. Hooman, Numerical study of melting performance enhancement for PCM in an annular enclosure with internal-external fins and metal foams, Int. J. Heat Mass Transf. 150 (2020), 119348.

[7] H.B. Mahood, M.S. Mahdi, A.A. Monjezi, A.A. Khadom, A.N. Campbell, Numerical investigation on the effect of fin design on the melting of phase change material in a horizontal shell and tube thermal energy storage, J. Energy Storage 29 (2020), 101331.

[8] H. Shabgard, C.W. Robak, T.L. Bergman, A. Faghri, Heat transfer and exergy analysis of cascaded latent heat storage with gravity-assisted heat pipes for concentrating solar power applications, Sol. Energy 86 (2012) 816–830.

[9] K. Nithyanandam, R. Pitchumani, Design of a latent thermal energy storage system with embedded heat pipes, Appl. Energy 126 (2014) 266–280.

[10] Hu. Bo-wen, Qian Wang, Zhen-Hua Liu, Fundamental research on the gravity assisted heat pipe thermal storage unit (GAHP-TSU) with porous phase change materials (PCMs) for medium temperature applications, Energy Convers. Manag. 89 (2015) 376–386.

[11] Nourouddin Sharifi, Amir Faghri, Theodore L. Bergman, Charles E. Andraka, Simulation of heat pipe-assisted latent heat thermal energy storage with simultaneous charging and discharging, Int. J. Heat Mass Transf. 8 (2015) 170–179.

[12] Chunjian Pan, Natasha Vermaak, Carlos Romero, Sudhakar Neti, Sean Hoenig, Chien-Hua Chen, Efficient optimization of a longitudinal finned heat pipe structure for a latent thermal energy storage system, Energy Convers. Manag. (2017) 93–105.

[13] D. Tolga Pirasaci, Yogi Goswami, Influence of design on performance of a latent heat storage system for a direct steam generation power plant, Appl. Energy 162 (2016) 644–652.

[14] H.J. Xu, C.Y. Zhao, Thermal performance of cascaded thermal storage with phase-change materials (PCMs). Part I: steady cases, Int. J. Heat Mass Transf. 106 (2017) 932–944.

[15] H.J. Xu, C.Y. Zhao, Thermal performance of cascaded thermal storage with phase-change materials (PCMs). Part II: unsteady cases, Int. J. Heat Mass Transf. 106 (2017) 945–957.

[16] Zhang-Jing Zheng, Xu. Yang, Ming-Jia Li, Eccentricity optimization of a horizontal shell-and-tube latent-heat thermal energy storage unit based on melting and melting-solidifying performance, Appl. Energy 220 (2018) 447–454.

[17] S.Saeed Mostafavi Tehrani, Robert A. Taylor, Pouya Saberi, Gonzalo Diarce, Design and feasibility of high temperature shell and tube latent heat thermal energy storage system for solar thermal power plants, Renew. Energy 96 (2016) 120–136.

[18] Soheila Riahi, Wasim Y. Saman, Frank Bruno, Martin Belusko, N.H.S. Tay, Performance comparison of latent heat storage systems comprising plate fins with different shell and tube configurations, Appl. Energy 212 (2018) 1095–1106.

[19] H. Xu, Y. Wang, X. Han, Analytical considerations of thermal storage and interface evolution of a PCM with/without porous media, Int. J. Numer. Methods Heat Fluid Flow 30 (2019) 373–400.

[20] V.G. Choudhari, A.S. Dhoble, S. Panchal, Numerical analysis of different fin structures in phase change material module for battery thermal management system and its optimization, Int. J. Heat Mass Transf. 163 (2020), 120434.

[21] A.N. Desai, A. Gunjal, V.K. Singh, Numerical investigations of fin efficacy for phase change material (PCM) based thermal control module, Int. J. Heat Mass Transf. 147 (2020), 118855.

[22] K. Mekrisuh, S. Giri, Udayraj, D. Singh, D. Rakshit, Optimal design of the phase change material based thermal energy storage systems: efficacy of fins and/or nanoparticles for performance enhancement, J. Energy Storage 33 (2021), 102126.

[23] M.T. Luu, D. Milani, M. Nomvar, A. Abbas, A design protocol for enhanced discharge exergy in phase change material heat battery, Appl. Energy 265 (2020), 114801.

[24] Y. Wang, A. Barde, A. Jin, R.E. Wirz, System performance analyses of sulfur-based thermal energy storage, Energy 195 (2020), 116996.

[25] L. Tang, Y. Zhou, S. Zheng, G. Zhang, Exergy-based optimisation of a phase change materials integrated hybrid renewable system for active cooling applications using supervised machine learning method, Sol. Energy 195 (2020) 514–526.

[26] M. Qu, M. Lu, Z. Li, X. Song, J. Chen, D. Ziviani, J.E. Braun, Thermal energy storage based (TES-based) reverse cycle defrosting control strategy optimization for a cascade air source heat pump, Energy Build. 219 (2020), 110014.

[27] T.F. Edgar, K.M. Powell, Energy intensification using thermal storage, Curr. Opin. Chem. Eng. 9 (2015) 83–88.

[28] Hafiz Muhammad Ali, Adeel Arshad, Muhammad Mansoor Janjua, Wajahat Baig, Uzair Sajjad, Thermal performance of LHSU for electronics under steady and transient operations modes, Int. J. Heat Mass Transf. 127 (2018) 1223–1232.

[29] W. Cole, K. Powell, T. Edgar, in: Optimization and Advanced Control of Thermal Energy Storage Systems 28, 2012, pp. 81–99.

[30] Gianluca Serale, Massimo Fiorentini, Alfonso Capozzoli, Paul Cooper, Marco Perino, Formulation of a model predictive control algorithm to enhance the performance of a latent heat solar thermal system, Energy Convers. Manag. 173 (2018) 438–449.

[31] F. Ghani, R. Waser, T.S. O'Donovan, P. Schuetz, M. Zaglio, J. Wortischek, Non-linear system identification of a latent heat thermal energy storage system, Appl. Therm. Eng. 134 (2018) 585–593.

[32] Minh Tri Luu, Dia Milani, Mobin Nomvar, Ali Abbas, Dynamic modelling and analysis of a novel latent heat battery in tankless domestic solar water heating, Energy Build. 152 (2017) 227–242.

[33] Mohamad Salameh, Stephen Wilke, Ben Schweitzer, Peter Sveum, Said Al-Hallaj, Mahesh Krishnamurthy, Thermal state of charge estimation in phase change composites for passively cooled lithium-ion battery packs, IEEE Trans. Ind. Appl. 54 (2018) 426–436.

[34] Tilman Barz, Dominik Seliger, Klemens Marx, Andreas Sommer, Sebastian F. Walter, Hans Georg Bock, Stefan Körkel, State and state of charge estimation for a latent heat storage, Control. Eng. Pract. 72 (2018) 151–166.

[35] D.W. Peaceman, H.H. Rachford Jr., The numerical solution of parabolic and elliptic differential equations, J. Soc. Ind. Appl. Math. 3 (1955) 28–41.

[36] C. Pan, N. Vermaak, X. Wang, et al., A fast reduced model for a shell-and-tube based latent heat thermal energy storage heat exchanger and its application for cost optimal design by nonlinear programming, Int. J. Heat Mass Transf. 176 (2021) 121479.

[37] J. Wang, Q. Zhang, Y. Yu, X. Chen, S. Yoon, Application of model-based control strategy to hybrid free cooling system with latent heat thermal energy storage for TBSs, Energy Build. 167 (2018) 89–105.

[38] F. Ni, Z. Zheng, Q. Xie, X. Xiao, Y. Zong, C. Huang, Enhancing resilience of DC microgrids with model predictive control based hybrid energy storage system, Int. J. Electr. Power Energy Syst. 128 (2021) 106738.

[39] D. Mariano-Hernández, L. Hernández-Callejo, A. Zorita-Lamadrid, O. Duque-Pérez, F. Santos García, A review of strategies for building energy management system: model predictive control, demand side management, optimization, and fault detect & diagnosis, J. Build. Eng. 33 (2021), 101692.

[40] H.S. Stone, An efficient parallel algorithm for the solution of a Tridiagonal linear system of equations, J. ACM 20 (1973) 27–38.

[41] M.A. Ammar, A. Jasim, M. Sohif, S. Kamaruzzaman, E. Bashir, A.M. Munther, Experimental and numerical study of solidifying phase-change material in a triplex-tube heat exchanger with longitudinal/triangular fins, Int. Commun. Heat Mass Transfer 90 (2018) 73–84.

[42] D. Zhao, G. Tan, Numerical analysis of a shell-and-tube latent heat storage unit with fins for air-conditioning application, Appl. Energy 138 (2015) 381–392.

[43] Z. Liao, C. Xu, Y. Ren, F. Gao, X. Ju, X. Du, A novel effective thermal conductivity correlation of the PCM melting in spherical PCM encapsulation for the packed bed TES system, Appl. Therm. Eng. 135 (2018) 116–122.

[44] S.S. Mostafavi Tehrani, Y. Shoraka, G. Diarce, R.A. Taylor, An improved, generalized effective thermal conductivity method for rapid design of high temperature shell-and-tube latent heat thermal energy storage systems, Renew. Energy 132 (2019) 694–708.

[45] K.A.R. Ismail, C.L.F. Alves, M.S. Modesto, Numerical and experimental study on the solidification of PCM around a vertical axially finned isothermal cylinder, Appl. Therm. Eng. 21 (2001) 53–77.

[46] C. Pan, J. Charles, N. Vermaak, C. Carlos, et al., Efficient modeling of phase change material solidification with multidimensional fins, Int. J. Heat Mass Transf. 115 (2017) 897–909.

[47] C. Pan, J. Charles, N. Vermaak, C. Carlos, et al., Experimental, numerical and analytic study of unconstrained melting in a vertical cylinder with a focus on mushy region effects, Int. J. Heat Mass Transf. 124 (2018) 1015–1024.

[48] C. Pan, N. Natasha Vermaak, C. Carlos Romero, S. Neti, S. Hoenig, C. Chen, R. Bonner, Cost estimation and sensitivity analysis of a latent thermal energy storage system for supplementary cooling of air cooled condensers, Appl. Energy 224 (2018) 52–68.

[49] Z. Liu, Z. Zengyi Wang, C. Ma, An experimental study on heat transfer characteristics of heat pipe heat exchanger with latent heat storage. Part I: Charging only and discharging only modes, Energy Convers. Manag. 47 (2006) 944–966.

[51] N.A.M. Amin, M. Belusko, F. Bruno, M. Liu, Optimizing PCM thermal storage systems for maximum energy storage effectiveness, Sol. Energy 86 (2012) 2263–2272.

[52] N.H.S. Tay, M. Belusko, F. Bruno, An effectiveness-NTU technique for characterising tube-in-tank phase change thermal energy storage systems, Appl. Energy 91 (2012) 309–319.